https://doi.org/10.18524/1810-4215.2024.37.313462

IMPLICATIONS OF PHOTON–AXION OSCILLATIONS ON X-RAY OBSERVATIONS OF THE COMA CLUSTER

Y.Sahai[1], L.Zadorozhna[1,2], O.Prikhodko[1], D.Malyshev[3], A.Tugay[1], N.Pulatova[4,5]
[1] Faculty of Physics, Taras Shevchenko National University of Kyiv, Ukraine
[2] Niels Bohr Institute, University of Copenhagen, Denmark
[3] Institut für Astronomie und Astrophysik Tübingen, Universität Tübingen, Germany
[4] Main Astronomical Observatory of the NAS of Ukraine, Kyiv, Ukraine
[5] Max-Planck-Institut für Astronomie, Heidelberg, Germany
e-mail: lidiia.zadorozhna@knu.ua

ABSTRACT. Axion-like particles (ALPs) emerge as predictions from various extensions of the Standard Model, standing out as plausible candidates for dark matter. Axions are thought to be produced when light passes through regions of magnetic fields. This positions astrophysical environments as prime sites for their production and subsequent detection. However, establishing precise constraints on axion parameters remains challenging, primarily due to the limited understanding of astrophysical magnetic fields. The Coma cluster is notable for being the sole cluster where the profile of magnetic field strength has been relatively accurately determined using Faraday Rotation Measures. We examined the X-ray spectrum of the Coma galaxy cluster using data from the XMM-Newton observatory. We combined data from eight XMM-Newton observations conducted between 2000 and 2005, spanning a $40' \times 40'$ area centered on the Coma cluster, totaling 343.8 ks. The X-ray spectrum of the ICM was characterized by modeling it with emissions from a single-temperature hot plasma. Furthermore, we explored the potential impact of photon-to-ALP conversion on the spectrum of the Coma cluster. Our investigation encompassed a range of parameters – the coupling constant and the axion mass, focusing on regions that have not yet been excluded. For the selected axion parameters, the primary impact on the spectrum could occur at high energies exceeding 5 keV. Analysis of the limited statistics gathered in this study indicates that the excluded parameter space for ALPs, based on X-ray observations of the Coma cluster, lies above the following values: $g_{a\gamma} < 5 \cdot 10^{-13}\,\mathrm{GeV}^{-1}$, $m_a < 1 \cdot 10^{-12}\,\mathrm{eV}$ with 95% probability.

Keywords: axion, clusters of galaxies, intergalactic plasma, X-ray radiation.

АНОТАЦІЯ. Аксіоноподібні частинки виникають як передбачення розширень Стандартної моделі, виокремлюючись як потенційні кандидати на роль темної матерії. Вважається, що аксіони формуються під час проходження світла через магнітні поля, що робить астрофізичне середовище ключовим місцем для їхнього утворення та можливого виявлення. Однак точне встановлення обмежень на параметри аксіонів залишається складною задачею, переважно через обмежене розуміння астрофізичних магнітних полів. Скупчення Кома привертає увагу тим, що воно єдине, де профіль напруженості магнітного поля відносно точно визначений за допомогою вимірювань обертання Фарадея. Ми дослідили рентгенівський спектр скупчення галактик Кома, використовуючи дані обсерваторії XMM-Newton. Для цього об'єднали дані 8 спостережень XMM-Newton з області розміром $40' \times 40'$ із центром у скупченні Кома, проведених у період з 2000 по 2005 рік, із загальною тривалістю 343,8 кс. Рентгенівський спектр внутрішньокластерного середовища був змодельований як випромінюваня однотемпературної гарячої плазми. Ми вивчали можливий вплив фотон-аксіонної конверсії на спектр кластера Кома. Ми розглянули параметри — константу зв'язку та масу аксіону, зосереджуючись зокрема на тих їх величинах, які досі залишалися невиключені. Для вибраних параметрів аксіонів їхній основний внесок у спектр може спостерігатися при високих енергіях, що перевищують 5 кеВ. Аналіз обмеженої статистики, зібраної у цьому дослідженні, показує, що простір параметрів для аксіоноподібних частинок, який є виключеним на підставі рентгенівських спостережень скупчення Коми, лежить вище за наступні значення: $g_{a\gamma} < 5 \cdot 10^{-13}\,\text{ГеВ}^{-1}$, $m_a < 1 \cdot 10^{-12}\,\text{еВ}$ з ймовірністю 95%.

Ключові слова: аксіон, скупчення галактик, міжгалактична плазма, рентгенівське випромінювання

1. Introduction

1.1. Exploring ALPs in astrophysics

Axions are hypothetical particles originally proposed as a solution to the strong CP-problem (Peccei, 1977a; Peccei, 1977b). Almost immediately, these particles were identified as prime candidates for dark matter (Weinberg, 1978; Wilczek, 1978). Today, we discuss a wider family of axion-like particles (ALPs) that share the main properties of axions: they are very light (much lighter than even a neutrino) and interact with photons when traversing regions of magnetic fields, via the term (Malyshev, 2018; Raffelt, 1988):

$$\mathcal{L}_{\gamma a} = -\frac{1}{4} g_{\gamma a} F_{\mu\nu} \tilde{F}^{\mu\nu} a = g_{\gamma a} \mathbf{E} \cdot \mathbf{B}\, a\,, \qquad (1)$$

where a is a pseudo-scalar axion field, $F_{\mu\nu}$ is the electromagnetic field strength, $\tilde{F}_{\mu\nu} \equiv \frac{1}{2}\varepsilon_{\mu\nu\rho\sigma}F^{\rho\sigma}$ is the electromagnetic dual, $\mathbf{E}$ and $\mathbf{B}$ are the electric and magnetic field strengths, respectively, and $g_{\gamma a}$ is the photon-axion coupling. Natural Lorentz-Heaviside units with $\hbar = c = 1$ are used throughout this article.

A variety of search strategies can be used depending on the ALP mass. ALPs can be detected through astrophysical observations or laboratory experiments, where photon-ALP oscillations occur in the presence of a magnetic field. These oscillations generate distinct features in the spectra of astrophysical objects. Photon-to-ALP conversion is expected to cause detectable energy-dependent distortions in the X-ray or γ-ray spectra of sources within or behind galaxy clusters (Conlon, 2016; Davies, 2023; Hochmuth, 2007; Malyshev, 2018; Meyer, 2013; Mirizzi, 2008; Reynolds, 2020). The absence of ALP imprints on photon signals from astronomical sources has been crucial in establishing constraints on the axion mass and coupling constant (O'Hare, 2020).

1.2. X-ray-ALP conversion in the cluster magnetic field

The propagation of a photon (A_x, A_y) with energy E along z-axis is described by (Hochmuth, 2007; Malyshev, 2018)

$$[E - i\partial_z - M(m_a, g_{\gamma a}, B_\perp)]\,\mathbf{A} = \mathbf{0}, \qquad (2)$$

where

$$\mathbf{A} \equiv \begin{pmatrix} A_x \\ A_y \\ a \end{pmatrix},$$

and $M(m_a, g_{a\gamma}, B_\perp)$ is the mixing matrix. The primary components of the mixing matrix, concerning keV photons traveling through the galaxy cluster environment are:

$$M = \begin{pmatrix} \Delta_{pl} & 0 & \Delta_{a\gamma}\cos\phi \\ 0 & \Delta_{pl} & \Delta_{a\gamma}\sin\phi \\ \Delta_{a\gamma}\cos\phi & \Delta_{a\gamma}\sin\phi & \Delta_a \end{pmatrix}, \qquad (3)$$

where $\cos\phi = \mathbf{B}_\perp \cdot \mathbf{e}_x / B_\perp = \sqrt{1-\sin^2\phi}$. Elements of the matrix Eq. (3) are given by:

$$\Delta_{a\gamma} = \frac{1}{2} g_{a\gamma} B_\perp \simeq$$

$$\simeq 7.6 \cdot 10^{-7} \left(\frac{g_{a\gamma}}{5 \cdot 10^{-13}\mathrm{GeV}^{-1}}\right) \left(\frac{B_\perp}{\mu\mathrm{G}}\right) \mathrm{pc}^{-1},$$

$$\Delta_a = -\frac{m_a^2}{2E} \simeq$$

$$\simeq -1.95 \cdot 10^{-3} \left(\frac{m_a}{5 \cdot 10^{-12}\mathrm{eV}}\right)^2 \left(\frac{E}{\mathrm{keV}}\right)^{-1} \mathrm{pc}^{-1},$$

$$\Delta_{\rm pl} = -\frac{\omega_{\rm pl}^2}{2E} \simeq$$

$$\simeq -1.1 \cdot 10^{-4} \left(\frac{E}{\mathrm{keV}}\right)^{-1} \left(\frac{n_e}{10^{-3}\,\mathrm{cm}^{-3}}\right) \mathrm{pc}^{-1},$$

where $\omega_{\rm pl}^2 = 4\pi\alpha n_e/m_e$ is the plasma frequency of the medium, n_e is the electron density and $\alpha \equiv e^2/(4\pi) = 1/137$ the fine-structure constant with e the electron charge.

$$\omega_{\rm pl} = e\left(\frac{n_e}{m_e}\right)^{1/2} = 1.17 \cdot 10^{-12} \left(\frac{n_e}{10^{-3} cm^{-3}}\right)^{1/2} \mathrm{eV}.$$

If axions exist, magnetic fields cause photons to convert into them with the strength of the interaction, controlled by $g_{a\gamma}$.

The probability of the photon-axion conversion is proportional to the magnetic field, perpendicular to the line of sight:

$$P_{\gamma a} \approx 3 \cdot 10^{-5} \left(\frac{B_\perp}{\mu\mathrm{G}} \frac{L}{10\,\mathrm{kpc}} \frac{g_{a\gamma}}{5 \cdot 10^{-13}\,\mathrm{GeV}^{-1}}\right)^2,$$

where L is the magnetic field coherent length. Here we have normalized the quantities to typical parameters relevant to the galaxy cluster.

1.3. Coma cluster

The Coma cluster (Abell 1656) has been extensively studied across various wavelengths as a galaxy cluster with a hot gas composition. Located approximately 99 Mpc from the observer, with a redshift of $z = 0.0231$, the Coma cluster consists of over 10^3 galaxies. This virialized structure possesses a mass ranging from 10^{14} to 10^{15} $M_\odot$ and extends over spatial scales of more than 1 Mpc (Bower, 2013). The intracluster medium (ICM) within the Coma cluster emits diffuse X-ray radiation primarily through thermal bremsstrahlung, with a typical temperature of $T \sim 10^8\,\mathrm{K}$ and a number density in the range of $n_e \sim 10^{-1} - 10^{-3}\,\mathrm{cm}^{-3}$ (Chen, 2007).

The celestial size of the Coma cluster extends over more than 2° in the sky, with its ICM being an extended X-ray source larger than $45'$.

Both radio and X-ray observations suggest turbulence and disruption within the intergalactic plasma (Churazov, 2012; Schuecker, 2004). Moreover, the behavior of transport processes is closely linked to the configuration of local magnetic field. The presence of substructures within the Coma ICM, particularly gas fluctuations arising from galaxy cluster collisions, highlights the intricate nature of the ICM.

The Coma cluster stands out as one of the few clusters whose magnetic field strength profile has been measured. The primary method for probing a cluster's magnetic fields is through Faraday rotation measure (RM). These fields are intimately connected with the plasma and can pervade its internal structure. Their properties often indicate a stochastic and turbulent nature. Generally, the beta-profile is employed for gas density, with a corresponding profile for the magnetic field. The radial distribution of electrons in the Coma cluster is described by $n_e(r) = n_0[1 + (r/r_c)^2]^{-3\beta/2}$, where $n_0 = 3.44 \cdot 10^{-3}\,\mathrm{cm}^{-3}$, $r_c = 291\,\mathrm{kpc}$, and $\beta = 0.75$ (Bonafede, 2010; Łokas, 2003), while the magnetic field profile follows $B(r) = B_0[n_e(r)/n_0]^{\eta}$, where $B_0 = 5.2\,\mu\mathrm{G}$ and $\eta = 0.67$ (Bonafede, 2010).

2. Data analysis

2.1. XMM-Newton X-ray spectrum

We analyzed observation data files for the Coma cluster from the XMM-Newton X-ray observatory. The observations included the following ObsIDs: 0124711401, 0153750101, 0300530101, 0300530301, 0300530401, 0300530501, 0300530601, and 0300530701, with a total exposure time of 343.8 ksec. We studied the combined MOS1/MOS2 spectra from the central region $40' \times 40'$ using the `Xspec` package. In our spectral analysis, we did not perform background subtraction because the object's size exceeds the field of view, making it impossible to select an appropriate region for background spectrum estimation. To account for residual calibration uncertainties in XMM-Newton observations, we added 1% systematic error.

The resulting **base model fit** (see Table 1) consists of the thermal radiation from the plasma `apec_3` within the Coma cluster, along with various astrophysical components such as Solar System plasma `apec_1`, hot interstellar plasma `apec_2`, and the cosmic X-ray background `powerlaw_1`. Additionally, it includes the hydrogen column density for absorption `phabs`, as well as instrumental backgrounds featuring a smooth continuum `powerlaw` and line-like `gaussian` features. Refs. (Malyshev, 2022; Zadorozhna, 2023) provide comprehensive lists of the most significant instrumental and astrophysical lines essential for modeling the XMM-Newton background.

2.2. Photon-to-ALP conversion simulation

We used the publicly available `AlPro` (Axion-Like PROpagation) (Matthews, 2022) code in Python designed to solve the equations of motion for a photon-ALP beam, accounting for the mixing between photon and ALP states.

We assumed that most of the X-ray photons that travel a sufficient distance and in a strong enough magnetic field to oscillate into axions are born in the central region of the cluster. The initial parameters for running the code were chosen as follows: the magnetic field profile and amplitude as described in subsection *1.3*, and the cluster radius was set to 1.5 Mpc. We divided the cluster into 50 randomly distributed domains, with sizes ranging from 2 to 32 kpc. The magnetic field's orientation varied randomly in the photon polarization plane within each domain, while the magnetic field amplitude remained constant in each domain. Each run of the code generated a curve depicting the probability of photon survival as it travels from the center of the Coma cluster (see Figures 1, 2). Significant contributions from conversions at the given ALP parameters occur at energies higher than 5 keV.

For the ALP parameters $g_{a\gamma} = 5 \cdot 10^{-13}\,\mathrm{GeV}^{-1}$ and $m_a = 5 \cdot 10^{-12}\,\mathrm{eV}$, the conversion probability does not exceed 1% as can be seen from Figure 1. Each curve was transformed into a multiplicative ALPs model and then multiplied by the **base model** (see Table 1). The fitting results for curves with these parameters are summarized in Table 2. In Table 1, the columns **fit 1**, **fit 3**, **fit 5**, and **fit 11** present the detailed fitting results as examples. For the ALP parameters $g_{a\gamma} = 6 \cdot 10^{-13}\,\mathrm{GeV}^{-1}$ and $m_a = 3 \cdot 10^{-12}\,\mathrm{eV}$, the conversion probability remains below 10%, as illustrated in Figure 2.

Figure 3 presents the spectrum with various model fits. The line colors in Figure 3 match the curve colors in Figure 2. These colored curves were used as a multiplicative ALPs model to fit the data and construct the correspondingly colored lines in Figure 3.

2.3. Bounds on ALPs

Detecting photon-axion oscillations in the X-ray thermal spectrum of a cluster is challenging due to the presence of spectral lines and complexities in background modeling. Our analysis found no significant

No	Model Comp.	Parameter Unit	**Value base model fit**	**Value base model+ALPs fit 1**	**Value base model+ALPs fit 3**	**Value base model+ALPs fit 5**	**Value base model+ALPs fit 11**
1	apec_1	kT, keV	0.307 ± 0.018	0.307 ± 0.018	0.307 ± 0.018	0.307 ± 0.018	0.307 ± 0.0182
2	apec_1	Abundance	1.000 frozen	1.000 frozen	1.000 frozen	1.000 frozen	1.000 frozen
4	apec_1	Redshift	0.0 frozen	0.0 frozen	0.0 frozen	0.0 frozen	0.0 frozen
5	apec_1	norm, cm^{-3}	$(8.278 \pm 1.941) \cdot 10^{-4}$	$(8.282 \pm 2.010) \cdot 10^{-4}$	$(8.285 \pm 1.941) \cdot 10^{-4}$	$(8.29 \pm 1.941) \cdot 10^{-4}$	$(8.278 \pm 1.942) \cdot 10^{-4}$
6	phabs	n_H, 10^{22} atoms cm^{-2}	$(1.502 \pm 0.491) \cdot 10^{-2}$	$(1.502 \pm 0.491) \cdot 10^{-2}$	$(1.502 \pm 0.492) \cdot 10^{-2}$	$(1.502 \pm 0.492) \cdot 10^{-2}$	$(1.502 \pm 0.492) \cdot 10^{-2}$
7	pl_1	PhoIndex	1.478 ± 0.021	1.478 ± 0.021	1.478 ± 0.022	1.478 ± 0.022	1.478 ± 0.022
8	pl_1	$\mathrm{ph\,cm^{-2}\,s^{-1}\,sr^{-1}\,keV^{-1}}$	$(2.450 \pm 0.249) \cdot 10^{-2}$	$(2.450 \pm 0.249) \cdot 10^{-2}$	$(2.450 \pm 0.249) \cdot 10^{-2}$	$(2.450 \pm 0.249) \cdot 10^{-2}$	$(2.450 \pm 0.249) \cdot 10^{-2}$
9	apec_2	kT, keV	1.002 ± 0.040	1.002 ± 0.040	1.002 ± 0.040	1.002 ± 0.040	1.002 ± 0.040
10	apec_2	Abundance	1.000 frozen	1.000 frozen	1.000 frozen	1.000 frozen	1.000 frozen
11	apec_2	Redshift	0.0 frozen	0.0 frozen	0.0 frozen	0.0 frozen	0.0 frozen
12	apec_2	norm, cm^{-3}	$(6.333 \pm 1.282) \cdot 10^{-4}$	$(6.333 \pm 1.282) \cdot 10^{-4}$	$(6.331 \pm 1.282) \cdot 10^{-4}$	$(6.335 \pm 1.282) \cdot 10^{-4}$	$(6.333 \pm 1.283) \cdot 10^{-4}$
13	apec_3	kT, keV	7.658 ± 0.140	7.671 ± 0.140	7.675 ± 0.140	7.678 ± 0.140	7.664 ± 0.139
14	apec_3	Abundance	0.542 ± 0.063	0.542 ± 0.063	0.544 ± 0.064	0.542 ± 0.064	0.542 ± 0.063
15	apec_3	Redshift	0.0231 frozen	0.0231 frozen	0.0231 frozen	0.0231 frozen	0.0231 frozen
16	apec_3	norm, cm^{-3}	$(7.658 \pm 0.908) \cdot 10^{-2}$	$(7.658 \pm 0.908) \cdot 10^{-2}$	$(7.658 \pm 0.908) \cdot 10^{-2}$	$(7.658 \pm 0.908) \cdot 10^{-2}$	$(7.658 \pm 0.908) \cdot 10^{-2}$
17	ALPs_1	$g_{a\gamma}$, GeV^{-1}	–	$5 \cdot 10^{-13}$	$5 \cdot 10^{-13}$	$5 \cdot 10^{-13}$	$5 \cdot 10^{-13}$
18	ALPs_1	m_a, eV	–	$5 \cdot 10^{-12}$	$5 \cdot 10^{-12}$	$5 \cdot 10^{-12}$	$5 \cdot 10^{-12}$
		$\chi^2/d.o.f.$	1926.78/1936	1928.97/1936	1924.78/1939	1921.19/1936	1926.78/1939
		P(H0)	30.0%	28.8%	31.1%	33.2%	30.0%

Table 1: Model parameters of the combined MOS1/MOS2 spectrum extracted from the central region of the Coma cluster. The column labeled **Value base model fit** displays a set of parameters for the complex model `apec_1 + phabs*(powerlaw_1+apec_2+apec_3)` with the addition of an instrumental background. The columns labeled **Value base model+ALPs fit 1**, **Value base model+ALPs fit 3**, **Value base model+ALPs fit 5**, and **Value base model+ALPs fit 11** present parameters from the previous model with an additional ALPs component (apec_1 + phabs*(powerlaw_1+apec_2+apec_3))*ALPs, including the contribution of instrumental background.

Table 2: Summary of the fitting results. The Fit column denotes the number of attempts made to approximate the spectrum using the complex model with the previously generated ALP model incorporated, corresponding to the curves in Figure 1. Columns labeled χ^2/d.o.f. and P(H0) show the chi-squared test results and the null hypothesis probability, respectively.

Fit	χ^2/d.o.f.	P(H0)
1	1928.97/1936	28.8%
2	1925.07/1939	31.0%
3	1924.78/1939	31.1%
4	1926.44/1939	30.2%
5	1921.19/1939	33.2%
6	1924.68/1939	31.2%
7	1927.34/1939	29.7%
8	1927.82/1939	29.4%
9	1928.08/1939	29.3%
10	1924.03/1939	31.6%
11-19	1926.78/1939	30.0%
20	1924.35/1939	31.1%

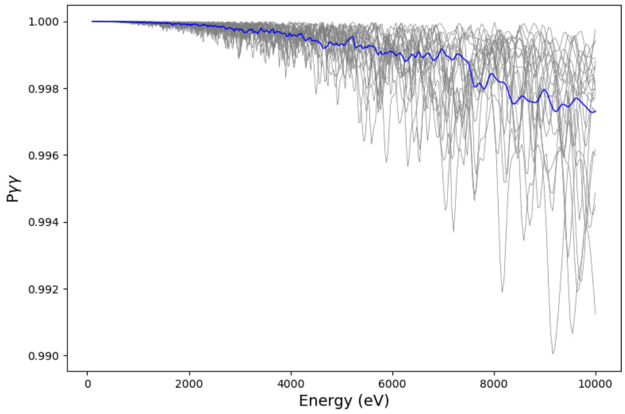

Figure 1: The photon survival probability when traversing the Coma cluster is shown for 20 different realizations of the cluster's magnetic field in **gray lines**. All realizations maintain the same amplitude and radial profile of the magnetic field. They differ only in the random orientation of the magnetic field to the photon polarization plane and the sizes of the domains in which the field remains constant. The gray curves fluctuate to such an extent that they nearly merge into a continuous area. The **blue line** illustrates the conversion probability averaged over these 20 realizations. The ALP parameters used are $g_{a\gamma} = 5 \cdot 10^{-13}\,\mathrm{GeV}^{-1}$ and $m_a = 5 \cdot 10^{-12}\,\mathrm{eV}$ for all curves.

deviations from the thermal spectrum, thus constraining the ALP parameter space. We scanned the parameter area for the axion-photon coupling constant $g_{a\gamma} \in [5 \cdot 10^{-13}\ \mathrm{GeV}^{-1}; 3 \cdot 10^{-12}\ \mathrm{GeV}^{-1}]$ and ALPs mass $m_a \in [1 \cdot 10^{-12}\ \mathrm{eV}; 5 \cdot 10^{-12}\ \mathrm{eV}]$ with a 10% step for each parameter and conducted 20 trials for each parameter pair. The results are represented by a color gradient in Figure 4: white indicates a 0% probability of exclusion, while blue indicates a 100% probability of exclusion. A parameter pair is excluded with 95% probability if 19 out of 20 tests show degradation of the baseline spectrum.

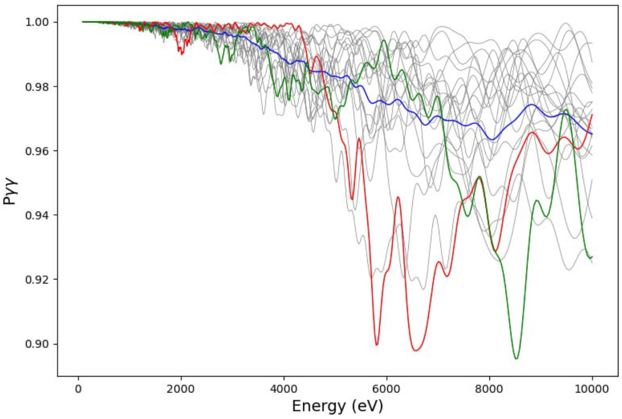

Figure 2: The photon survival probability through the Coma cluster is shown for 20 magnetic field realizations (**gray lines, green line, red line**), which differ in magnetic field orientation and domain sizes but share the same amplitude and radial profile. The average over these 20 realizations conversion probability is depicted by the **blue line**. The ALP parameters used are $g_{a\gamma} = 6 \cdot 10^{-13}\,\mathrm{GeV}^{-1}$ and $m_a = 3 \cdot 10^{-12}\,\mathrm{eV}$ for all curves.

Our assessment is limited by a 1% systematic error from residual calibration uncertainties in XMM-Newton observations. We did not take into account statistical errors due to limited observation time. Additionally, our limits may be overestimated because of the modest attempts for each pair of parameters, which we plan to address in future work. Nonetheless, our results are consistent with existing bounds and even improve upon them. It is important to note, however, that existing analyses are not optimized for ALP searches.

Notably, within the above parameter range, a significant increase in the null hypothesis probability was observed in one of the random realizations of the magnetic field for the ALP parameters $g_{a\gamma} = 6 \cdot 10^{-13}\,\mathrm{GeV}^{-1}$ and $m_a = 3 \cdot 10^{-12}\,\mathrm{eV}$. The probability rose to 88% from the base model's 30%. The photon survival probability curve corresponding to this fit is shown in Figure 2 as a red line. Additionally, Figure 2 also includes a green line representing the photon survival curve for which the fit has the lowest null hypothesis probability of just 0.08%.

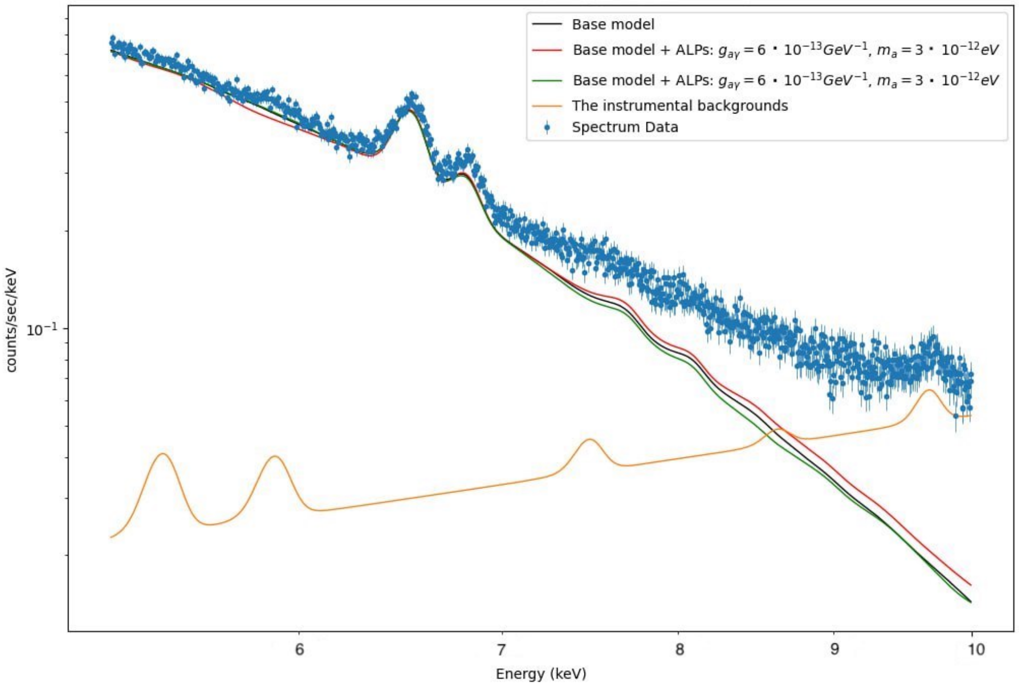

Figure 3: XMM-Newtom/MOS spectrum extracted from Coma cluster central region. The fitting using the base model is represented by a **black** line. The base model + ALPs with parameters $g_{a\gamma} = 6 \cdot 10^{-13}\,\mathrm{GeV}^{-1}$ and $m_a = 3 \cdot 10^{-12}\,\mathrm{eV}$, and the magnetic field realization that yields the highest null hypothesis probability 88% from our trials, is shown in **red**. The fit using the base model + ALPs with the same parameters, but with the realization that gives the lowest null hypothesis probability 0.08%, is depicted in **green**. The instrumental backgrounds (smooth continuum powerlaw and line-like gaussian features) is illustrated by the **yellow** line.

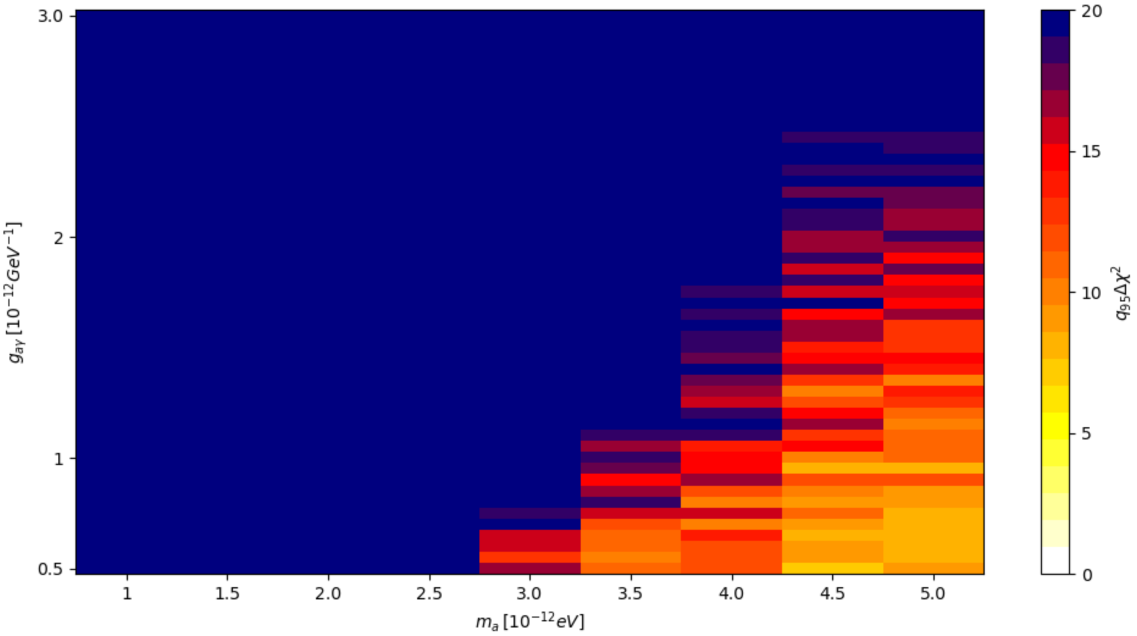

Figure 4: χ^2 change and ALP exclusion regions. The colors illustrate the difference between the best-fit χ^2 for the base model and the base + ALPs model for the Coma cluster XMM-Newton/MOS spectrum fit.

3. Conclusion

Based on X-ray observations of the Coma cluster, the excluded parameter space for ALPs is constrained to $g_{a\gamma} < 5 \cdot 10^{-13}\,\mathrm{GeV}^{-1}$ for $m_a < 1 \cdot 10^{-12}\,\mathrm{eV}$.

The study of X-ray emission from clusters and its connection to axions is promising, as data from space missions continue to improve. The first observational data from XRISM (The X-Ray Imaging and Spectroscopy Mission) has been published, offering greater precision with the Resolve Soft X-ray Spectrometer's 7 eV resolution. Additionally, new radio observations and the increased number of radio sources will enhance Faraday rotation measurements of galaxy clusters' magnetic fields, providing better constraints on ALP parameters.

Acknowledgements. Lidiia Zadorozhna's work is supported by a Scholars at Risk Denmark Fellowship for Scholars from Ukrainian Universities (SARU Fellowship) at the University of Copenhagen.

This research was made with the support of the Center for the Collective Use of Scientific Equipment "Laboratory of High Energy Physics and Astrophysics" of Taras Shevchenko National University of Kyiv.

References

Bonafede A. et al.: 2010, *A&A*, **513**, A30, 1002.0594.
Bower R.: 2013, Clusters of Galaxies. In: Oswalt, T.D., Keel, W.C. (eds) Planets, Stars and Stellar Systems, (Springer, Dordrecht).
Chen Y. et al.: 2007, *A & A*, **466**, 805.
Churazov E. et al.: 2012, *MNRAS*, **421**, 1123.
Conlon J.P., Powell A.J., & Marsh M.C.D.: 2016, *PhysRevD*, **93**, 123526.
Davies J., Meyer M., & Cotter G.: 2023, *PhysRevD*, **107**, 083027.
Hochmuth K.A. & Sigl G.: 2007, *PhysRevD*, **76**, 123011.
Łokas E.L. & Mamon G.A.: 2003, *MNRAS*, **343**, 401.
Malyshev D. et al.: 2018, *arXiv e-prints*, arXiv: 1805.04388.
Malyshev D., Moulin E., & Santangelo A.: 2022, *PhysRevD*, **106**, 123020.
Matthews J.H. et al.: 2022, *ApJ*, **930**, 90.
Meyer M., Horns D., & Raue M.: 2013, *PhysRevD*, **87**, 035027.
Mirizzi A., Raffelt G.G., & Serpico P.D.: 2008, *Axions,* **741**, 115.
O'Hare C.: 2020, Zenodo, https://cajohare. github.io/ AxionLimits/.
Peccei R.D. & Quinn H.R.: 1977a, *PhysRevD*, **16**, 1791.
Peccei R.D. & Quinn H.R.: 1977b, *PhysRevL*, **38**, 1440.
Raffelt G. & Stodolsky L.: 1988, *PhysRevD*, **37**, 1237.
Reynolds C.S. et al.: 2020, *ApJ*, **890**, 59.
Schuecker P. et al.: 2004, *A&A*, **426**, 387.
Weinberg S.: 1978, *PhysRevL*, **40**, 223.
Wilczek F.: 1978, *PhysRevL*, **40**, 279.
Zadorozhna L. et al: 2023, *OAP*, **36**, 36.